Interannual Variability of Temperature, Water Vapor, and Clouds in the Tropical Tropopause Layer

Aodhan Sweeney[1] and Qiang Fu[1]

[1]University of Washington, Department of Atmospheric Sciences.
Corresponding author: Aodhan Sweeney (aodhan@uw.edu)

Key Points:

- Variability of temperature, water vapor at 83 hPa, and cirrus in the tropical tropopause layer is dominated by stratospheric processes
- Tropical cold point tropopause height covaries with both stratospheric and tropospheric temperatures
- The extent of stratospheric versus tropospheric control of this interannual variability changes based on season

Abstract

Water vapor and cirrus clouds in the Tropical Tropopause Layer (TTL) are important for the climate and are largely controlled by temperature in the TTL. On interannual timescales, both stratospheric and tropospheric modes of variability affect temperatures in the TTL. In this study, we use satellite observations to investigate the explained variance in cold point temperature (CPT), 83 hPa water vapor (WV83), and TTL cirrus cloud fraction (TTLCCF) over the equatorial region (15°N - 15°S) using a multiple linear regression (MLR) model where predictors are stratospheric and tropospheric modes of variability. The MLR model can explain 68%, 60%, and 52% of the variance in CPT, WV83, and TTLCCF. The model suggests that these variables are dominated by stratospheric 'top-down' processes associated with the Quasi-Biennial Oscillation (QBO) and Brewer Dobson Circulation (BDC) as opposed to tropospheric 'bottom-up' processes associated with the El Nino Southern Oscillation (ENSO) and the Madden-Julian Oscillation (MJO). Although cold point temperature is controlled by 'top-down' mechanisms, the cold point tropopause height is related to both 'top-down' stratospheric and 'bottom-up' tropospheric processes. Our MLR model explains more variance during boreal winter. We also investigate how these modes of variability correlate with zonal mean temperature, water vapor, and cloud fraction globally in the upper troposphere and lower stratosphere (UTLS) and find significant relationships between clouds and the modes of variability.

Plain Language Summary

Between the tropical troposphere and stratosphere, water can exist as either vapor or ice phases. The partitioning of this water between vapor and ice is largely controlled by the coldest temperatures in this region, which on interannual timescales could be modulated by both stratospheric and tropospheric processes. Here we show that 68%, 60%, and 52% of the interannual variance in cold point temperature, water vapor at 83 hPa, and ice clouds in this region can be explained using a multiple linear regression (MLR) model, where the predictors are known stratospheric and tropospheric processes. Stratospheric processes are much more important in controlling these interannual variances, but notably, the height of the cold point is controlled by both stratospheric and tropospheric processes. The explained variances also depend

on seasons, with more variance explained during boreal winter. Finally, we check how these predictors correlate with temperature, water vapor, and cloud fraction globally in the upper troposphere and lower stratosphere (UTLS) and find significant relationships throughout the globe.

1 Introduction

Water vapor and cirrus clouds in the Tropical Tropopause Layer (TTL) are important for surface climate. Stratospheric water vapor impacts stratospheric ozone and Earth's radiative budget, and its concentration is regulated by the coldest temperatures in the TTL (Mote et al., 1996; Forster and Shine 1999; Kirk-Davidoff et al., 1999; Holton and Gettelman, 2001; Fueglistaler and Haynes, 2005; Solomon et al., 2010; Joshi et al., 2010; Flury et al., 2012a; Ding & Fu, 2018; Randel and Park, 2019). Temperatures in the TTL control water vapor through the formation of thin and extensive ice clouds referred to as TTL cirrus clouds. These clouds are important for the local radiative heating rate in the TTL (McFarquhar et al., 2000; Dinh et al., 2010) which may impact the TTL upwelling (Corti et al, 2006; Yang et al, 2010) and feedback to temperatures there (Fu et al., 2018). TTL cirrus clouds might also likely contribute a warming effect on the surface and may be important for interannual fluctuations in surface climate (Zhou et al., 2014). Despite their importance, climate models neither precisely nor accurately simulate TTL cirrus cloud fraction and stratospheric water vapor concentrations (Gettelman et al., 2010; Randel and Jensen, 2013; Hardiman et al., 2015; Wang and Fu, 2021).

Because of the cold temperatures and high relative humidity of the TTL, small variations in the TTL temperatures dictate how much water vapor can transit into the stratosphere versus how much is turned into ice and sediments out of the TTL (Jensen 1996; Jensen et al., 2013; Randel and Jensen, 2013). The TTL itself extends from the level of zero net radiative heating to the maximum height where clouds still exist (~14.5 to ~18.5 km) and is located between the troposphere and stratosphere (Holton et al. 1995; Gettelman and Forster, 2002; Fu et al, 2007; Fueglistaler et al, 2009). Temperature variability in this region is thus a result of both stratospheric and tropospheric processes (Davis et al., 2013; Randel and Wu, 2015; Tseng and Fu, 2017b; Lu et al., 2020). On interannual timescales the temperature, water vapor, and clouds in the TTL exhibit extreme variability driven by stratospheric modes including the Quasi-Biennial Oscillation (QBO) and Brewer Dobson circulation (BDC) and tropospheric modes including the El Nino Southern Oscillation (ENSO) and Madden-Julian Oscillation (MJO) (Virts and Wallace 2010; Eguchi and Kodera, 2010; Liang et al., 2011; Davis et al 2013; Li and Thompson 2013; Virts and Wallace 2014; Ding and Fu 2017; Tseng and Fu 2017a; Tseng and Fu 2017b; Ye et al; 2018; Sweeney et al., 2023). Gravity waves have also been shown to be contemporaneous with low cold point tropopause temperatures (CPTs) and TTL cirrus clouds (Grise and Thompson 2013; Kim and Alexander 2015; Podglajen et al., 2016; Kim et al., 2016; Podglajen et al., 2018; Chang and L'Ecuyer 2020; Bramberger et al., 2022).

A fundamental question regarding the interannual variability remains: to what extent are these observed fluctuations governed by stratospheric processes, acting via a 'top-down' mechanism, versus tropospheric processes, acting via a 'bottom-up' mechanism (Fu, 2013; Ding and Fu, 2018)? This study attempts to answer this question by examining the explained variance based on a multiple linear regression (MLR) model, where predictors are the tropospheric and stratospheric modes of variability (Dessler et al., 2013; Dessler et al., 2014; Tseng and Fu, 2017b; Wang et al., 2019). This MLR model is fitted to timeseries of interannual variations in CPT, 83 hPa water vapor (WV83) and ozone ($O_3$83), and TTL cirrus cloud fraction (TTLCCF)

averaged over 15°S-15°N, obtained from observations by GPS radio occultations, the Microwave Limb Sounder (MLS), and the CALIOP instrument, respectively. Results show much stronger susceptibility of these variables to stratospheric processes, suggesting that the interannual variability of these variables is governed by a 'top-down' mechanism. The interannual variability of $O_3$83 is also examined here, motivated by a recent study (Match and Gerber, 2022) showing that tropospheric expansion under global warming reduces tropical lower stratospheric ozone. Results show that the skill of this MLR model depends on season (Li and Thompson, 2013; Martin et al., 2021; Sweeney et al., 2023). We also investigate how the modes of large-scale variability correlate with upper-tropospheric and lower-stratospheric temperature, water vapor, and cloud fraction globally, and find significant correlations throughout the globe.

2 Data

2.1 Temperature from Radio Occultations

Temperature data comes from Global Positioning System Radio Occultation (GPS-RO) measurements from the COSMIC-1 and 2 as well as the MetOp-A, B, and C satellites, archived at the University Corporation for Atmospheric Research. Data was preprocessed using the level 2 WetPrf product from June 2006 to December of 2021 (Sweeney and Fu, 2021). These GPS-RO temperature profiles have high accuracy (less than 0.1 K). They have high vertical resolution (~0.5 km) in the TTL, but coarser horizontal resolution of about 200 km (Kursinski et al, 1997; Kuo et al, 2004; Zeng et al, 2019).

2.2 Clouds from CALIPSO

The main instrument used to identify clouds in this study is the Cloud-Aerosol Lidar with Orthogonal Polarization (CALIOP) lidar (Winker et al, 2010). CALIOP can provide information of cloud layers with optical depth as small as 0.01 or less, ideal for TTL cirrus cloud identification. We use the Level 2 V4.2 5-km Merged Layer Products using only nighttime measurements from June of 2006 to December of 2021 to avoid the solar contamination on the lidar signals (Thorsen et al., 2013; Thornberry, 2017). The primary quantity derived from the CALIPSO data is the cloud fraction, which is defined as the number of detections of a cloud divided by the total number of observations in each 2.5°x2.5° grid cell at a given level. TTL cirrus in this study is defined as the clouds with bases above 14.5 km (Tseng and Fu, 2017a; Tseng and Fu, 2017b). Our metrics for All clouds consider all clouds including the TTL cirrus. Positive cloud identifications here require Cloud-Aerosol Distinction (CAD) values of greater than 30. This study uses an adapted version of the Level 2 V4.2 data for clouds above the lapse rate tropopause (Sweeney et al., 2023).

2.3 Microwave Limb Sounder

Water vapor and ozone data is obtained using the Microwave Limb Sounder (MLS) onboard the Aura Spacecraft. MLS measurements began in August 2004 and continue until present day. We use monthly mean Level 3 MLS values from June 2006 to December of 2021.

2.4 Indices of Physical Processes

The QBO index is defined using the monthly mean 10°S-10°N 50 hPa zonal wind from ERA5 (Hersbach et al., 2020). The QBO index has a two-month lead of the zonal winds to account for its descent from 50 hPa to the cold point tropopause (Dessler et al, 2013; Dessler et al 2014; Ding and Fu 2018; Tseng and Fu 2017b; Ye et al., 2018; Tian et al., 2019; Sweeney et al., 2023). The ENSO is the dominant mode of variability in the troposphere (Philander et al., 1989). Instead of using a traditional ENSO index, we use the 15°S-15°N 500 hPa temperature (T500) which is highly correlated with a three-month lead of the ENSO 3.4 index (r=0.79) and

captures how anomalous convection heats the troposphere (Dessler et al., 2013; Wang et al., 2019; Marsh and Garcia, 2007).

The BDC index is the tropopause upwelling between 15°S-15°N from the residual stream function (Rosenlof, 1995). The upwelling is calculated using the ERA5 reanalysis with 6-hourly data from 1979-2021 (Abalos et al., 2012). We define the tropopause upwelling by interpolating between pressure levels to match the seasonally varying CPT pressure identified from a GPS-RO derived climatology between 15°S-15°N. Noting that this upwelling can be impacted by both the QBO and T500, we regress out the combined impact of both from the upwelling using a MLR from 1979-2021.

The impact of the MJO is represented by the second principal component of the velocity potential index (Ventrice et al., 2013). Maximums in this MJO index are associated with peak MJO-related convection over the western Pacific and suppressed over the eastern Indian Ocean (Virts and Wallace, 2014; Tseng and Fu, 2017b). We also quantify the impact of gravity waves using the monthly mean gravity wave potential energy (E_P) diagnosed from each RO temperature profile (T_{Prof}) by finding the gravity wave temperature anomaly profiles (T_{GW}) (Alexander et al., 2008; Wang and Alexander, 2015; Luo et al., 2021). To define T_{GW}, we create 5° latitude x 20° longitude maps of tropical temperature profiles using 30-day time periods centered on each day in the record (Chang and L'Ecuyer, 2020). For each T_{Prof} we bilinearly interpolate the given day's background temperature map to the latitude and longitude of T_{Prof}, resulting in the background temperature profile ($T_{background}$). T_{GW} is defined as $T_{Prof} - T_{background}$. Because we use 30-day mean background temperature maps, the derived E_P will be contributed by all waves with time periods less than 30 days. We initially created the gravity wave index using E_P averaging over the 15°S-15°N TTL but found significantly greater correlations and more uniquely explained variance of target variables when we averaged E_P from 17-19 km over 10°-20° in both hemispheres. We thus define the GW index as the average gravity wave potential energy from 17-19 km over 10°S-20°S and 10°N-20°N.

3 Results

3.1 The Control of Interannual Variability on the Target Variables

This study attempts to quantify the impact of stratospheric and tropospheric modes of variability (Section 2.4) on the target variables (i.e., temperatures, water vapor, and cloud fractions) in the TTL. Figure 1 shows the climatological annual mean (1st row) and interannual standard deviations (2nd row) of TTL variables (as well as vertical temperature gradient). Interannual standard deviations are the standard deviations of monthly anomalies after removing the mean seasonal cycle. The solid (dashed) black line in each plot is the climatological mean cold point (lapse rate) tropopause height.

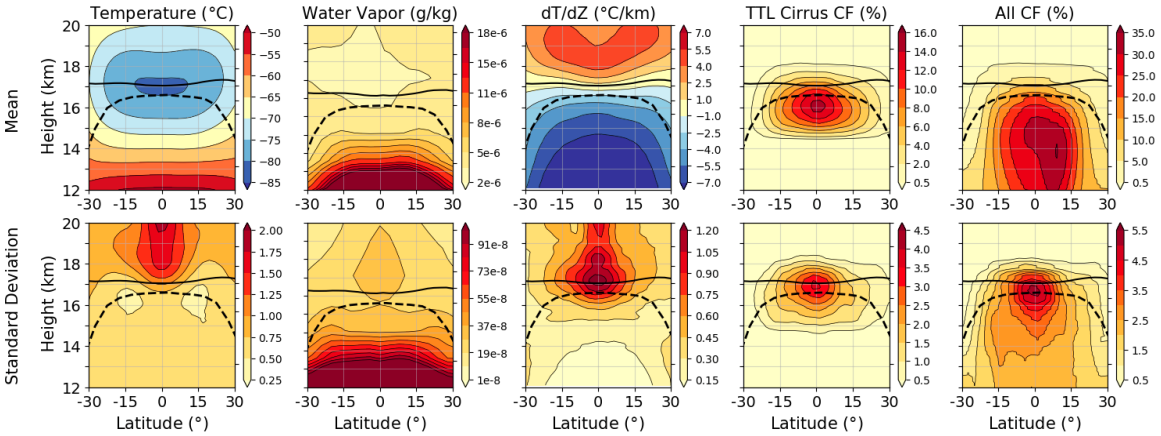

Figure 1: (Top) Climatological means of target variables in the upper troposphere and lower stratosphere. (Bottom) Interannual standard deviations of target variables. The solid (dashed) black line in all plots is the climatological mean cold point (lapse rate) tropopause.

The first panel of Fig. 1 shows the characteristically cold temperatures of the TTL (Fueglistaler et al., 2009). Water vapor carried into the stratosphere must pass these cold temperatures and thus reaches its minimum above the equatorial tropopause (Mote et al., 1996; Flury et al., 2012a). The magnitude of the vertical temperature gradient (dT/dZ) decreases with height throughout the troposphere and increases into the stratosphere. Changes in both temperature and dT/dZ are important for cirrus cloud formation (Kim et al., 2016; Tseng and Fu, 2017b; Chang and L'Ecuyer, 2020). Directly below the equatorial tropopause, TTL cirrus clouds reach their maximum and rarely occur in the stratosphere (Tseng and Fu, 2017a). The interannual standard deviation of temperature maximizes in the equatorial lower stratosphere (Randel and Wu, 2015). Large variability in cold point temperature occurs near the equator, resulting in peak stratospheric water vapor variability near the equatorial tropopause (Randel and Park, 2019). The elevated temperature variability near the tropopause is collocated with the increased TTL cirrus variability. Notably, peak cloud fraction variability is close to the cold point tropopause with significant variations occurring above the cold point, very much collocated with variance in dT/dZ (Tseng and Fu, 2017b).

Figure 2 shows how target variables correlate with different modes of variability except row 1 that shows the correlation with zonal-mean cold point tropopause temperature (CPT) averaged over 15°S-15°N. Although the CPT is not itself a mode of variability, it is critically important for both stratospheric water vapor (e.g., Randel and Jensen, 2013) and is highly correlated with TTL cirrus cloud fraction (Tseng and Fu, 2017b). CPT is highly correlated with temperatures above the cold point tropopause, suggesting that processes impacting CPT are tied to lower-stratospheric temperatures (Randel and Wu, 2015). CPT is also strongly correlated with stratospheric temperature throughout the globe, showing both QBO and BDC signatures (see Figure 4). Lower-stratospheric water vapor is highly correlated with the CPT (e.g., Randel and Jensen, 2013). Correlations between water vapor and CPT are transported throughout the stratosphere by the BDC (Brewer et al., 1949; Mote et al., 1996; Flury et al., 2012a; Flury et al., 2012b). Water vapor is also transported meridionally through the quasi-horizontal isentropic mixing between lower and higher latitudes (Randel and Park, 2019). CPT is strongly anticorrelated with TTL cirrus and All cloud fraction (CF) directly below the cold point tropopause. Two nodes of positive correlation between CPT and CF exist near the subtropical

lapse rate tropopause, the inverse of the correlation between CPT and temperature. The strong correlations between CPT and the target variables stress the temperature control of the partitioning of water between clouds and vapor in the TTL (Tseng and Fu, 2017b).

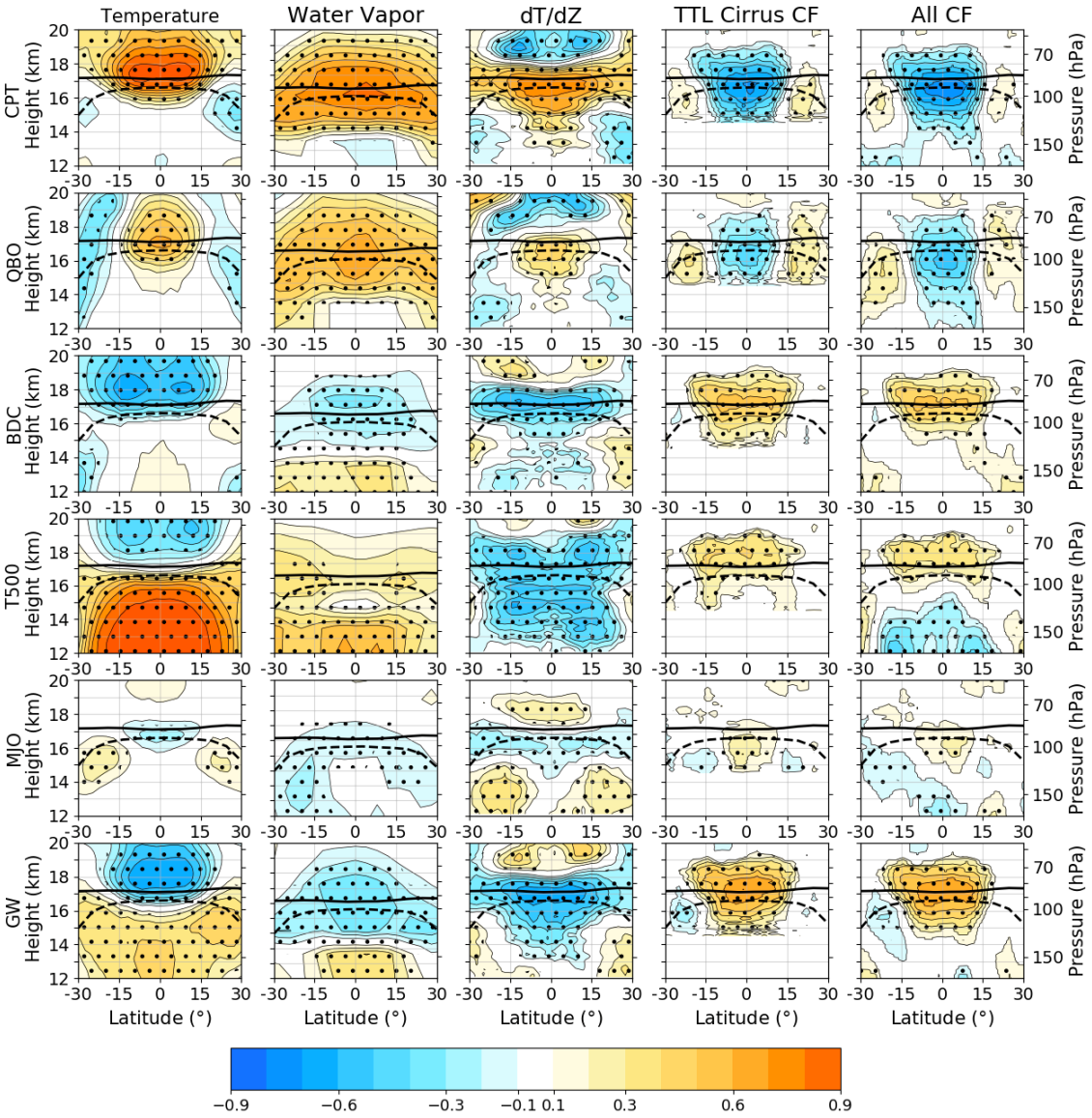

Figure 2: Correlations in tropical upper troposphere and lower stratosphere between target variable monthly anomalies and modes of large-scale variability except for row 1 that shows correlation between target variables and CPT averaged over 15°S-15°N. Stippling indicates significance at 95% confidence and the solid (dashed) black line is the climatological mean cold point (lapse rate) tropopause.

The QBO and temperature are correlated (anticorrelated) in the equatorial (subtropical) TTL due to the QBO's meridional circulation (Plumb and Bell, 1982; Baldwin et al., 2001; Pahlavan et al., 2021). The water vapor signal associated with the QBO shows peak correlation at the equatorial tropopause and is transferred to higher latitudes through isentropic mixing

(Randel and Park, 2019). The QBO correlations with CF mirror those with temperature. The subtropical cloud fraction correlations are weaker than the equatorial signal, which may be due to the weaker QBO-temperature correlation in the subtropics combined with this region's lower relative humidity. This may also contribute to the QBO's positive subtropical correlations in water vapor. QBO correlations with equatorial TTL cirrus CF are weaker than correlations with temperature, water vapor, and All CF. Significant QBO correlations with All CF reach depths of 12 km, well below the region of peak QBO power (Sweeney et al., 2023).

The BDC index used here is strongly anticorrelated with lower stratospheric temperatures (Mote et al., 1996; Plumb and Eluszkiewicz, 1999) and is strongly correlated with cloud fraction which maximizes directly above the equatorial cold point tropopause. Although clouds are infrequent in these regions, a substantial amount of cloud fraction variation occurs above the climatological mean cold point tropopause (see Fig. 1). The BDC is negatively correlated with water vapor in lower stratosphere, yet the correlation is weaker than the BDC correlation with temperature and cloud fraction. The response of target variables to the CPT appears to be a linear combination of the responses to QBO and BDC.

T500 is highly correlated with ENSO which cools lower-stratospheric temperatures by accelerating the BDC (Garfinkel and Hartmann 2008; Randel et al., 2009; Calvo et al., 2010). T500 also measures convective heating of the troposphere leading to strong positive correlations all the way up to the tropopause (Holloway and Neelin, 2007). Notably, T500 is not significantly correlated with CPT (Figure S1). ENSO is not correlated to zonal mean CPT due to the dipolar zonal impact near the tropopause (Randel et al., 2000; Scherllin-Pirscher et al., 2012). In Fig. 2 a weak significant correlation is found between T500 (and no correlation with ENSO 3.4) and lower-stratospheric water vapor, possibly due to its weak impact on zonal mean CPT, or a nonlinear relationship between ENSO and lower-stratospheric water vapor (Avery et al., 2017; Diallo et al., 2018; Garfinkel et al., 2021; Ziskin Ziv et al., 2022). T500 has significant correlations with cloud fraction above the tropopause, where temperature and dT/dZ correlations are strong (Davis et al., 2013).

Row 5 of Fig. 2 shows correlations of the MJO and target variables. The MJO impacts subseasonal variability of temperature and cloud fraction in the TTL (Virts and Wallace., 2014). The monthly timescale used in this study smooths some of the MJO variability. Further, the zonal mean MJO signal may cancel due to the MJO's strong moving dipole of active and inactive convection (Tseng and Fu, 2017b; Virts et al., 2010). Weak correlations between the MJO and the target variables are present.

Of all the modes of variability investigated, the GW index has the strongest correlations with cloud fraction and elicits a strong response in vertical temperature gradient near the tropopause. Like results of cirrus clouds and CPT, the cirrus cloud and GW index correlation pattern is akin to a linear combination of the QBO and BDC correlation pattern with cloud fraction. The QBO is driven by gravity waves (e.g., Pahlavan et al., 2021), and its impact on gravity wave potential energy is well documented (e.g., De La Torre, 2006). The equatorial upwelling associated with tropical waves induces a strong meridional circulation with upwelling (cold anomalies) near the equatorial tropopause and downwelling (warm anomalies) near the subtropical tropopause, related to the shallow branch of the BDC (Ortland and Alexander, 2014). This wave impact on the upwelling may cause similar correlation patterns of cirrus clouds and the GW and BDC.

We next use a multiple linear regression (MLR) model to quantify the explained variance in the 15°S-15°N average CPT, water vapor at 83 hPa (WV83), TTL cirrus cloud fraction

(TTLCCF) that is the total cloud fraction for all clouds with cloud base above 14.5 km (Tseng and Fu, 2017a; Tseng and Fu, 2017b). We also apply this MLR model to All Cloud Fraction (ALLCF) that is the total cloud fraction for all clouds with cloud top above 14.5 km regardless of cloud base height, cold point tropopause height (CPZ), and ozone concentrations at 83 hPa ($O_3$83). Although 15°S-15°N is close to the equator, it is where most of the variability in the target variables occurs (see Fig. 1). The predictors in this MLR model are the modes of variability and are described in 2.4. WV83 is lagged by one month with respect to other variables to account for transit time from the cold point tropopause height to 83 hPa. We choose to quantify the control of TTLCCF and ALLCF separately because TTLCCF may be more relevant for the water vapor dehydration in the TTL, while ALLCF is more relevant for the upwelling in the TTL and for the total energy budget of the tropics (Corti et al., 2006; Jensen et al., 2013; Sokol and Hartmann, 2020; Sweeney et al., 2023).

The explained variance is defined using the adjusted R^2, which accounts for artificially high R^2 due to potential collinearity in the MLR and is always less than the true R^2. The unique contribution of explained variance to the adjusted R^2 from each predictor is not possible if predictors are correlated. A correlation matrix among all predictors and target variables is provided in Figure S1. Although most of our predictors show no statistically significant relation over the period investigated, the GW index is highly correlated to the QBO, BDC, and T500 index. Further, insignificant weak correlations between predictors also exist. To account for this, we partition the adjusted R^2 into the unique contributions from the QBO, BDC, T500, and MJO by recursively adding each predictor to our MLR model while also permuting the order of addition, allowing for an estimate of unique explained variance (Lindeman et al., 1980). We note that this method is not perfect but provides an estimate of the unique variance contributed to the MLR from each mode of variability. After the unique explained variances are found for these four processes, the unique explained variance by GW is found by taking the difference between the adjusted R^2 before and after adding in the GW to the MLR model.

Figure 3 shows that 68%, 60%, 52%, 35%, 74%, and 56% of the variance in CPT, WV83, TTLCCF, ALLCF, CPZ, and $O_3$83 can be explained using this MLR model. 'Top-down' processes (i.e., the QBO and BDC) explain most of the variance captured by the MLR in all variables except CPZ. This model's ability explained TTLCCF variance varies strongly with height, explaining over 60% of the variance in TTL cirrus and All cloud fraction at 17 km (not shown). Increased explained variance at these higher levels may be due to the types of clouds at these altitudes (more mostly laminar tropopause cirrus) (Wang et al., 2019). This MLR model only captures a third of the ALLCF variance, so other processes must control its interannual variance. The GW index, which is significantly correlated with QBO, BDC and T500 (see Fig. S1), adds very little unique variance to the MLR, indicating that although the GW index is very well correlated with the target variables, its contribution is mostly explained by the QBO, BDC, and T500 indices.

Ozone concentrations in tropical lower stratosphere may decrease in the future due to the strengthening of the BDC but may also be depleted due to the expansion of the troposphere (Banerjee et al., 2016; Chiodo et al., 2018; Wang et al., 2020; Match and Gerber, 2022). We examined the correlations of 15°S-15°N 83hPa ozone concentrations ($O_3$83) from MLS with the predictors as well as other target variables considered (see Fig. S1). Interannual variations in $O_3$83 are very well correlated with equatorial tropopause height (r=-0.75). Increases in CPZ decrease lower stratospheric O_3 concentrations by mixing low O_3 tropospheric air with stratospheric air. Figure 3 shows that the MLR explains 56% of $O_3$83 variance. Of this explained

variance ~1/5 is contributed by T500 and another ~1/5 comes from the BDC while the remaining ~3/5 are explained by the QBO. Despite its important role in determining $O_3$83 interannual variability, QBO is less relevant for the future climate given its quasi-period characteristics and large uncertainties in its changes in response to climate (e.g., Butchart et al., 2020; Richter et al., 2020; Fu et al. 2020). Our results that both T500 and the BDC affect $O_3$83 are in alignment with a recent study claiming that both contribute future O_3 concentration changes in the tropical lower stratosphere (Match and Gerber, 2022).

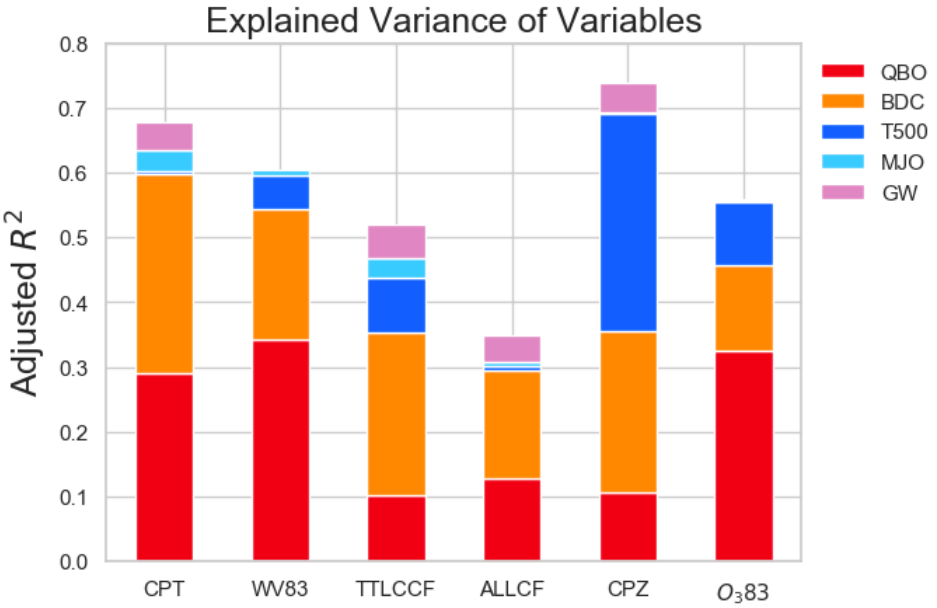

Figure 3: Adjusted R^2 from multiple linear regression model applied to target variables using modes of the large-scale variability as predictors. Colored sections indicate the estimated contribution to the adjusted R^2 from each predictor. The GW contribution here is that after removing contributions from BDC, QBO, T500, and MJO (see text).

We also investigate the power spectra of residual timeseries after variance captured from our model has been removed (Fig. S2). It is revealed that the CPT and WV83 still retain large interannual variations with spectral peaks at 2+ year periods. The residual TTLCCF and ALLCF power spectra are dominated by intraseasonal variability, with periods less than 9 months. This suggests that physical processes which control the residual variability in CPT and WV83 are different than those that control cloud fraction.

Tseng and Fu (2017b) stressed the importance of CPT in determining the TTLCCF. If we include CPT as a predictor in our MLR model for TTLCCF, the adjusted R^2 increases only slightly from 0.52 to 0.55. In other words, most of the CPT control of TTLCCF has already been included in our MLR, and the remaining variance in the TTLCCF timeseries is uncoupled from the CPT. This is not true for WV83 whose explained variance increases markedly by 15% (from 0.60 to 0.75) when including CPT as a predictor. This underscores the importance of the CPT in determining entry values of lower-stratospheric water vapor but suggests that the temperature control of TTLCCF is already captured by our MLR model. Figure S3 shows that the residual tropical CPT is still strongly correlated with lower-stratospheric temperatures throughout the globe, suggesting that the residual CPT variability is further largely controlled by 'top-down' processes that are not captured by our MLR model. The resemblance of this correlation map to

the BDC signal in lower stratospheric temperature shows that our BDC index is capturing only part of the BDC's importance for CPT. Although our BDC index maximizes the explained variance in the target variables, a similar pattern of strong correlations between the residual CPT and global stratospheric temperature is apparent when using a BDC index based on 100-hPa heat flux (Li and Thompson et al., 2013; Tseng and Fu, 2017b) to remove the BDC from the CPT (not shown).

A notable result of Fig. 3 is that although CPT is entirely dependent on stratospheric processes, CPZ has almost equal contribution from stratospheric and tropospheric processes. Figure 4 shows the correlations of CPT and CPZ averaged over 15°S-15°N with zonal mean temperature from 5-40 km obtained from the GPS-RO data. As suggested in Fig. 4, the CPT is controlled by the processes throughout the global stratosphere. The checkerboard pattern in the tropical stratosphere is due to the meridional circulation associated with the QBO. The anticorrelation above the equatorial cold point and the polar lower stratosphere is due to the BDC. Notably, the CPT is not significantly correlated with tropospheric temperatures anywhere. In contrast, CPZ is also highly correlated with temperature in the tropical upper troposphere. As tropospheric temperatures warm, the thermal expansion of the troposphere lifts the CPZ (Santer et al., 2003; Lorenz and DeWeaver, 2007; Lin et al., 2017). A strong BDC signal is also apparent in the CPZ and temperature correlation map. These correlation maps show that the temperature and height of the equatorial tropopause are impacted by different physical processes.

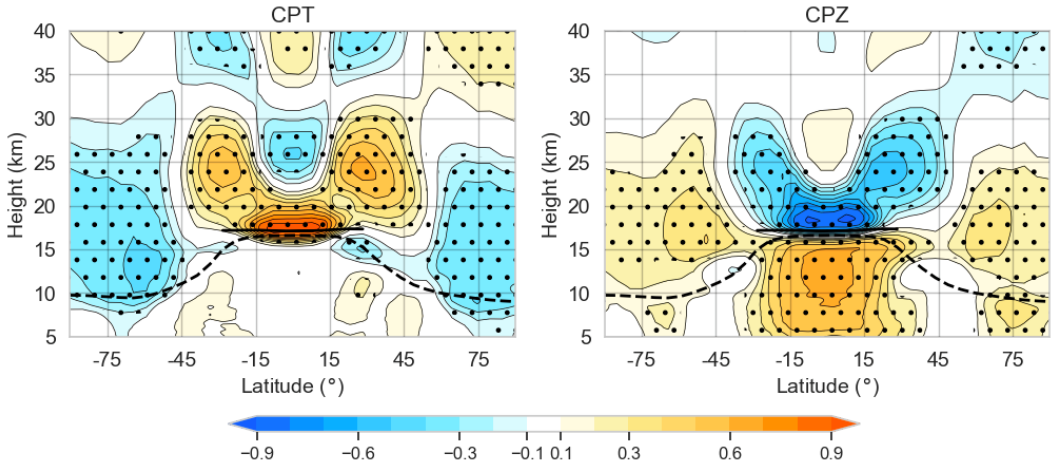

Figure 4: Correlation of cold point temperature (CPT) and height (CPZ) averaged over 15°S-15°N with zonal mean temperature globally from 5-40 km obtained from GPS-RO data. Stippling indicates significance at 95% confidence and the solid (dashed) black line is the climatological mean cold point (lapse rate) tropopause.

3.2 Seasonality

Figure 3 showed that a significant portion of the interannual variance in the target variables can be explained by the investigated modes of variability. A less studied aspect of the influence of these processes on the TTL is how their impact depends on season. Many studies have shown that the correlation between interannual variations in CPT and lower-stratospheric water vapor varies with season (Randel and Jensen, 2013; Randel and Park 2019, Lu et al., 2020). Seasonal changes in the tropical upwelling and the Asian monsoon also impact the seasonal variation in TTL cirrus clouds and stratospheric water vapor (Sunilkumar et al., 2010; Randel et al 2009; Abalos et al., 2012; Walker et al., 2015; Ueyama et al., 2015; Tseng and Fu, 2017b; Ueyama et al., 2018; Das and Suneeth, 2020). There is also evidence that the modes of

variability investigated impact the TTL differently throughout the year (Li and Thompson, 2013; Konopka et al., 2016; Tweedy et al., 2018; Martin et al., 2021; Sweeney et al., 2023).

The climatological mean and standard deviations of target variables for extended boreal winter (NDJFM) and summer (MJJAS) are shown in Figure 5. During NDJFM the TTL is colder, drier, and cloudier than in MJJAS. Standard deviations of interannual anomalies during boreal winter and summer are shown in the third and fourth rows of Fig. 5. NDJFM has more variability near the tropopause in all variables. Although the lower stratosphere is drier during NDJFM, standard deviations in lower-stratospheric water vapor are larger, especially over the equatorial tropopause. This may be tied to the increased temperature variance near the equatorial tropopause during boreal winter (see row 3 of Fig. 5) (Randel and Park, 2019). Peak standard deviations are still focused near the equatorial tropopause, suggesting that the 15°S-15°N TTL is still key to understanding their interannual variability.

Figure S4 shows correlation matrices between all target variables and predictors for both NDJFM and MJJAS separately. Like previous findings, we find a stronger correlation between WV83 and CPT during boreal winter compared to boreal summer (r=0.84 compared to r=0.65), which has been extensively reported (Randel and Jensen, 2013; Lu et al., 2020). Interestingly, we find that this seasonal variation is reversed for cloud fraction. CPT and cloud fraction have a weaker correlation during boreal winter (r=-0.63 for TTLCCF and r=-0.57 for ALLCF) compared to boreal summer (r=-0.7 for TTLCCF and r=-0.72 for ALLCF). Tseng and Fu (2017b) reported stronger correlations between CPT and cloud fraction closer to the tropopause. Given that the tropopause is lower during MJJAS and that cloud fractions are defined using a 14.5 km threshold, this may be a result of more near tropopause cirrus during MJJAS.

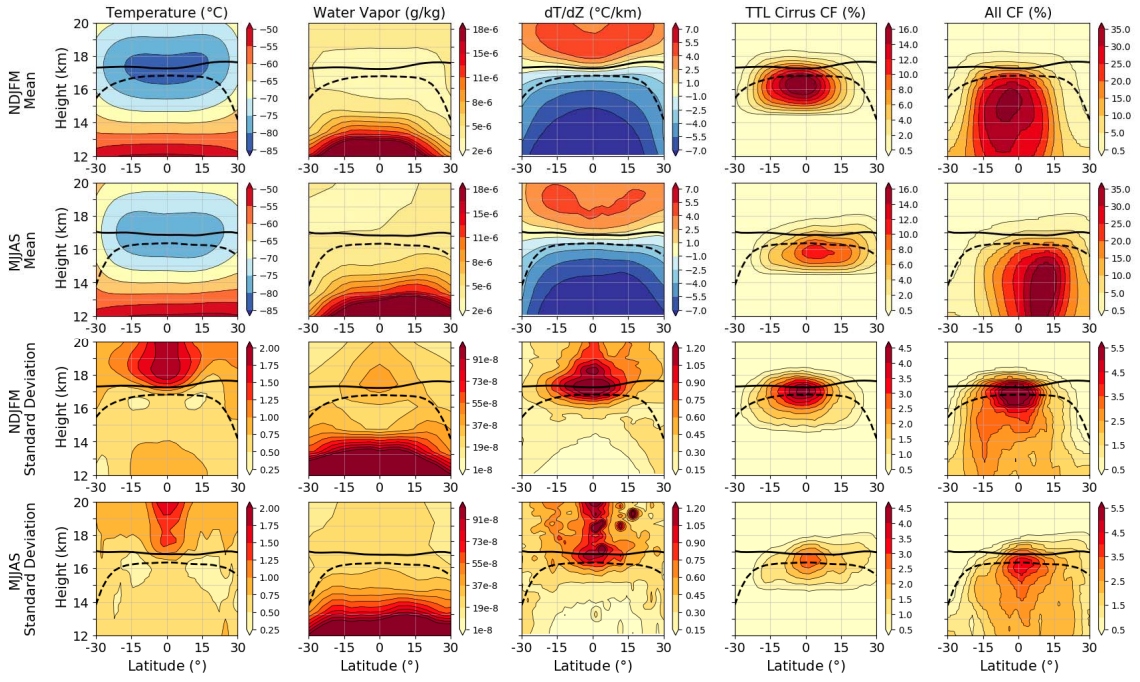

Figure 5: Seasonal means (rows 1 and 2) and interannual standard deviations (rows 3 and 4) of target variables split into NDJFM and MJJAS. The thick white line in all plots is the seasonal mean cold point tropopause height.

We next fit the MLR model to the interannual variations of 15°S-15°N target variables for both NDJFM and MJJAS individually in Figure 6. Note that the seasonal split reduces the data for each MLR by more than half, so partitioning of the variance is likely less reliable. The MLR predicts target variables slightly better during NDJFM than MJJAS (besides ALLCF). This increase in skill during boreal winter is mainly related to the BDC due to the much weaker BDC presence during boreal summer. Although the seasonal cycle in the BDC index has been removed, anomalies in the BDC index are weaker during MJJAS due to the decreased wave driving during southern hemisphere winter. The QBO exhibits a strong seasonality in correlation with TTLCCF (r=-0.26 in NDJFM and r=-0.37 in MJJAS), ALLCF (r=-0.25 in NDJFM and -0.52 in MJJAS), and $O_3$83 (r=0.43 in NDJFM and r=0.72 in MJJAS) explaining more CF variance during MJJAS. This is also true for CPT and WV83, but the seasonality is weaker. Sweeney et al. (2023) found that the zonal mean QBO signal in clouds is more zonally symmetric and propagates further into the troposphere from April-June, causing stronger QBO correlations with cloud fraction during MJJAS. The reason for this deeper QBO penetration depth during boreal spring and early summer is still not known. Further, the MJJAS TTL is less variable than that of NDJFM, so a given QBO signal should be more salient during this season. The 'bottom-up' processes contribute more explained variance during MJJAS. This may be due to the aliasing of the Boreal Summer Intraseasonal Oscillation into our MJO index, or indirectly capturing monsoon variability in our T500 index through its impact on tropospheric temperatures.

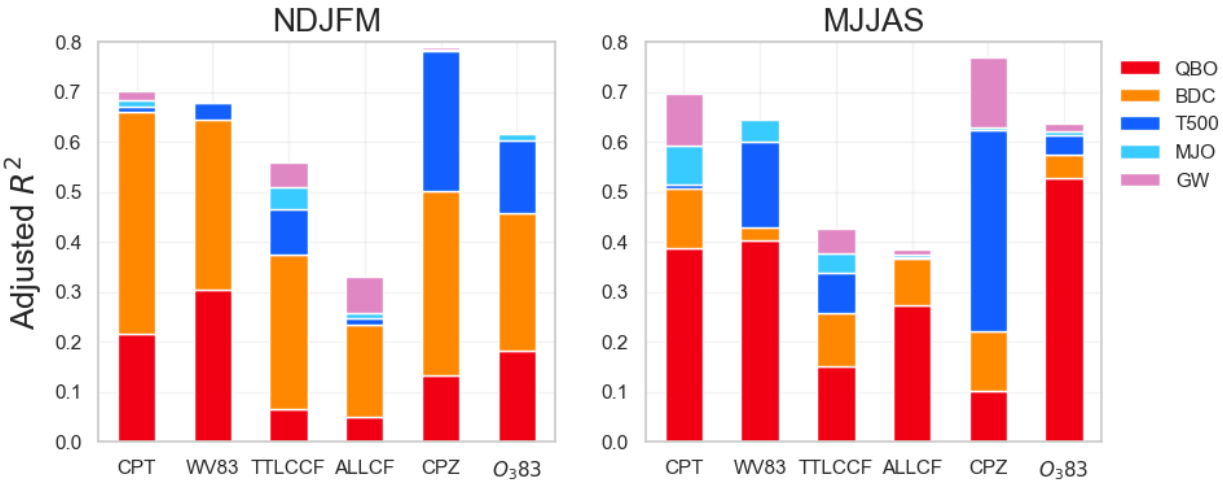

Figure 6: Adjusted R^2 from MLR model applied to target variables for NDJFM and MJJAS individually. Colored sections indicate the contribution to the adjusted R^2 from each predictor.

3.3 Impacts on the Global Upper Troposphere and Lower Stratosphere

The above sections show that a significant portion of the interannual variance in temperature, water vapor and clouds in the equatorial TTL can be explained by the QBO, BDC, and T500. Here we investigate the correlations of the target variables over the global upper troposphere and lower stratosphere (UTLS) with these modes of variability. Figure 7 shows the correlations between the monthly anomalies of zonal mean target variables in the UTLS from 80°S-80°N and the QBO, BDC, and T500. The QBO and T500 indices are described in section 2.4. The BDC index used in Fig. 7 is the cold point tropopause upwelling between 30°S-30°N after regressing out the impacts from T500 and QBO. We also include results using this BDC

index with a one-month lead (BDC1ml) to account for potential lags between the tropopause upwelling and high latitude downwelling associated with the BDC (Li and Thompson, 2013; Tseng and Fu, 2017b). We do not show results for TTL cirrus clouds as they are only defined in the tropics. Because we only use nighttime data from CALIPSO, correlations in the polar regions are based only on data during polar night. We exclude results related to the MJO due to its minimal global zonal mean impact, and gravity wave activity because of its difficulty in defining a globally relevant index.

The first row in Fig. 7 shows strong anticorrelations of the QBO with temperature with extend from the subtropics to ~50° in both hemispheres following the lapse rate tropopause height. Water vapor increases associated with warmer equatorial tropopause temperatures are transported globally. Cloud fraction correlations mirror those of temperature. A small but statistically significant increase in cloud fraction occurs in the Arctic which may suggest that the QBO has impacts on polar clouds during boreal winter, but this is not further investigated (Garfinkel and Hartmann, 2011; Yamazaki et al., 2020).

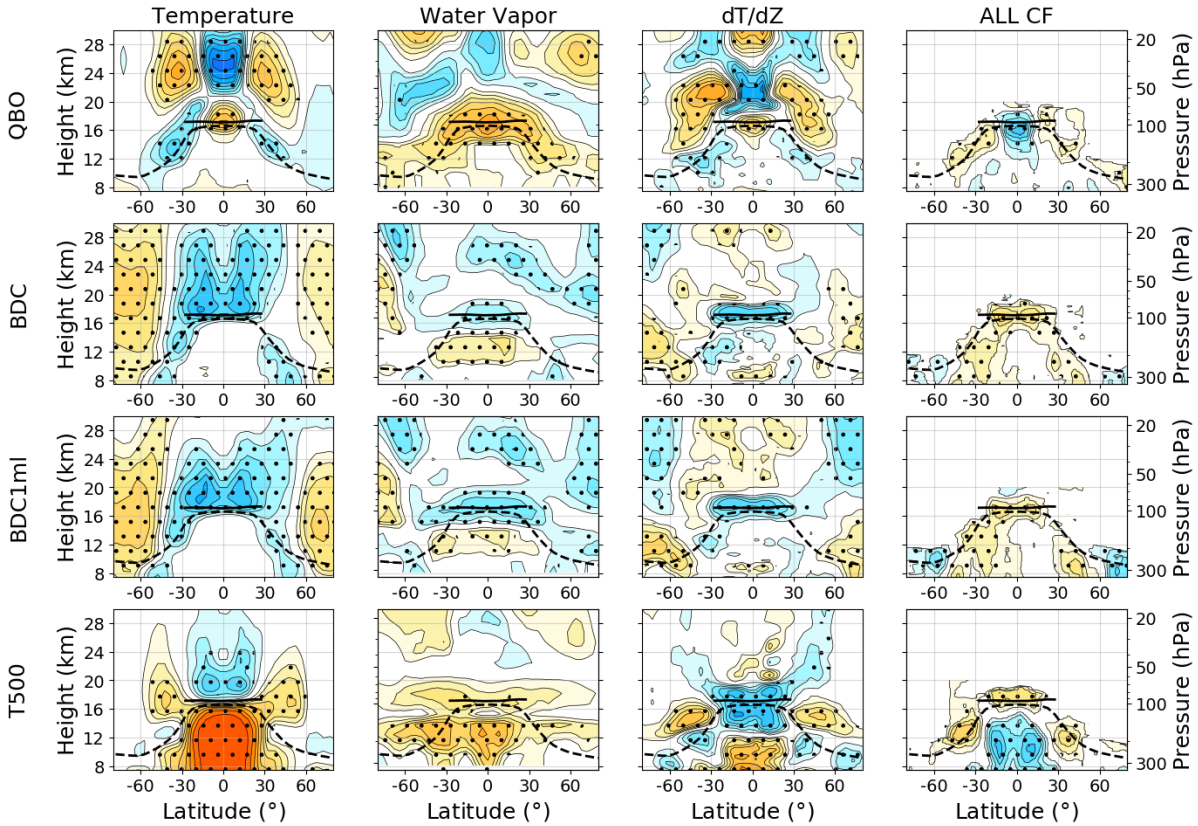

Figure 7: Correlations between the monthly anomalies of target variables in the global upper troposphere and lower stratosphere and modes of variability including QBO, BDC, BDC1ml and T500. BDC1ml is the BDC index with a one-month lead. Stippling indicates significance at 95% confidence and the solid (dashed) line is the cold point (lapse rate) tropopause height.

The BDC is significantly anticorrelated with temperature in the stratosphere equatorward of 40° and positively correlated poleward. The BDC anticorrelation with water vapor is weak throughout the global lower stratosphere except over the south pole. Cloud fraction correlations associated with the BDC are the inverse of those of temperature, with positive correlations

trailing the lapse rate tropopause. Using this BDC1ml index, correlations of the BDC and dT/dZ in the polar regions are closer to the lapse rate tropopause. The BDC1ml is also significantly correlated with Arctic and Antarctic clouds from 7-12 km. Li and Thompson (2013) showed that the BDC impacts both equatorial and Arctic high clouds during boreal winter. Here we show that this is also true with Antarctic high clouds, but the correlation is weaker. Note that we only use nighttime cloud fraction data from CALIPSO, so cloud fraction correlations in the polar regions are only representative of the winter response.

The final column in Fig. 7 shows the correlations of target variables with T500. As expected, strong correlations with temperature and water vapor throughout the tropical atmosphere are visible. The correlation with lower stratospheric temperature indicates a signature of the shallow branch of the Brewer-Dobson circulation. Increases in temperature and dT/dZ are anticorrelated with CF. CF near the tropopause increases from 50°S-50°N and is collocated with decreases in the vertical temperature gradient near the tropopause in these regions. We find no statistically significant correlation between polar clouds and T500 in either hemisphere. Figure 7 indicates that the correlation of cold point temperature averaged over 15°S-15°N with global zonal mean temperature shown in Fig.4 is a response to the QBO and BDC.

5 Conclusions

Stratospheric water vapor and TTL cirrus clouds are important for the Earth's radiative budget and are poorly constrained in climate models. Both exhibit large interannual variability, which is strongly correlated to the equatorial CPT, stressing the temperature control of the phase of water in the TTL (Jensen et al., 2013; Tseng and Fu, 2017b). Previous work shows that the QBO, BDC, and ENSO contribute to this interannual variability by modulating the thermodynamic environment of the TTL (e.g., Dessler et al., 2013; Davis et al., 2013; Randel and Wu, 2015). Here we investigate how these modes of variability, the MJO, and GW contribute to this interannual variability. To do this, we use a MLR model to explain the variance in CPT, WV83 and TTLCCF using these modes of variability as predictors. In addition, we also apply our MLR model to ALLCF, CPZ, and $O_3$83.

We find that 68%, 60%, 52%, 35%, 74%, and 56% of CPT, WV83, TTLCCF, ALLCF, CPZ, and $O_3$83 variance can be explained using this MLR model. The most important predictor for our cloud fraction is the BDC. The BDC index used here is the 15°S-15°N tropopause upwelling diagnosed from the residual stream function after regressing out the impacts of the QBO and T500 (Rosenlof, 1995). This BDC index's high correlation may be related to its capturing of tropical/subtropical wave activity which induces upwelling near the equatorial tropopause and downwelling in the subtropics and contributes to the shallow branch of the BDC (Abalos et al., 2012; Ortland and Alexander, 2014; Abalos et al., 2014). The GW index was strongly correlated to all target variables investigated, yet only marginally contributed to explained variance after considering QBO, BDC and T500. This suggests that although gravity wave activity is important for tropopause temperature and TTLCCF, its impact on interannual timescales can be considered though other modes of variability.

It is shown that explained variance of CPT, WV32, TTLCCF, and $O_3$83 is associated with stratospheric processes (see Figs. 2 and 3), suggesting that the interannual variability of the target variables is mostly controlled by 'top-down' processes. CPT was entirely controlled by stratospheric processes, while CPZ is controlled by near equal contributions from 'top-down' and 'bottom-up' processes. Analysis of the residual CPT variability shows that it is still well correlated to lower-stratospheric temperature. Adding the residual CPT timeseries into the MLR

model increases the explained variance of WV83 but only marginal increases in explained variance of cloud fractions, meaning remaining variance in TTLCCF is uncoupled from the CPT. It should be noted that the roles of BDC shown in Figs. 3 and 6 might be underestimated since part of the BDC shallow branch is included in T500 (Fig.7).

The modes of variability might impact the target variables differently based on the time of year (Li and Thompson, 2013; Konopka et al., 2016; Tweedy et al., 2018; Martin et al., 2021; Sweeney et al., 2023). The interannual variability of the target variables is confined to the equatorial region regardless of season (see Fig. 4). We applied our MLR model to extended boreal winter and summer individually. We find that more interannual variance is explained during NDJFM compared to MJJAS, which is largely due to the weakened BDC during boreal summer. The MJJAS MLR model was more dependent on "bottom-up" processes which may be related to the importance of convection to clouds and water vapor in the TTL during MJJAS (Ueyama et al., 2018).

Correlations between the QBO, BDC, and T500 and the target variables throughout the global UTLS were also investigated. Correlations in temperature are collocated with anticorrelations in CF. While previous studies have shown that the BDC can impact Arctic high clouds, this study shows that the BDC also impacts Antarctic high clouds during polar night (although the relationship is weaker in the Antarctic).

Acknowledgments

This research is supported by the NASA FINESST Grant 80NSSC22K1438 and NSF Grant AGS-2202812. We thank Prof. John M. Wallace for encouragement and valuable discussions.

Open Research

The code for this project is being held at https://github.com/AodhanSweeney/TTLVariability. The processed data will be held on zenodo and released at the time of publication.

References

Abalos, M., Randel, W. J., & Serrano, E. (2012). Variability in upwelling across the tropical tropopause and correlations with tracers in the lower stratosphere. *Atmospheric Chemistry and Physics*, *12*(23), 11505–11517. https://doi.org/10.5194/acp-12-11505-2012

Abalos, Marta, Randel, W. J., & Serrano, E. (2014). Dynamical Forcing of Subseasonal Variability in the Tropical Brewer–Dobson Circulation. *Journal of the Atmospheric Sciences*, *71*(9), 3439–3453. https://doi.org/10.1175/JAS-D-13-0366.1

549 Alexander, S. P., Tsuda, T., Kawatani, Y., & Takahashi, M. (2008). Global distribution of
550 atmospheric waves in the equatorial upper troposphere and lower stratosphere: COSMIC
551 observations of wave mean flow interactions. *Journal of Geophysical Research:*
552 *Atmospheres*, *113*(D24). https://doi.org/10.1029/2008JD010039
553 Avery, M. A., Davis, S. M., Rosenlof, K. H., Ye, H., & Dessler, A. E. (2017). Large anomalies
554 in lower stratospheric water vapour and ice during the 2015–2016 El Niño. *Nature*
555 *Geoscience*, *10*(6), 405–409. https://doi.org/10.1038/ngeo2961
556 Baldwin, M. P., Gray, L. J., Dunkerton, T. J., Hamilton, K., Haynes, P. H., Randel, W. J., et al.
557 (2001). The quasi-biennial oscillation. *Reviews of Geophysics*, *39*(2), 179–229.
558 https://doi.org/10.1029/1999RG000073
559 Banerjee, A., Maycock, A. C., Archibald, A. T., Abraham, N. L., Telford, P., Braesicke, P., &
560 Pyle, J. A. (2016). Drivers of changes in stratospheric and tropospheric ozone between year
561 2000 and 2100. *Atmospheric Chemistry and Physics*, *16*(5), 2727–2746.
562 https://doi.org/10.5194/acp-16-2727-2016
563 Bramberger, M., Alexander, M. J., Davis, S., Podglajen, A., Hertzog, A., Kalnajs, L., et al.
564 (2022). First Super-Pressure Balloon-Borne Fine-Vertical-Scale Profiles in the Upper TTL:
565 Impacts of Atmospheric Waves on Cirrus Clouds and the QBO. *Geophysical Research*
566 *Letters*, *49*(5), e2021GL097596. https://doi.org/10.1029/2021GL097596
567 Brewer, A. W. (1949). Evidence for a world circulation provided by the measurements of helium
568 and water vapour distribution in the stratosphere. *Quarterly Journal of the Royal*
569 *Meteorological Society*, *75*(326), 351–363. https://doi.org/10.1002/qj.49707532603

570 Butchart, N., Anstey, J. A., Kawatani, Y., Osprey, S. M., Richter, J. H., & Wu, T. (2020). QBO
571 Changes in CMIP6 Climate Projections. *Geophysical Research Letters*, *47*(7),
572 e2019GL086903. https://doi.org/10.1029/2019GL086903
573 Calvo, N., Garcia, R. R., Randel, W. J., & Marsh, D. R. (2010). Dynamical Mechanism for the
574 Increase in Tropical Upwelling in the Lowermost Tropical Stratosphere during Warm
575 ENSO Events. *Journal of the Atmospheric Sciences*, *67*(7), 2331–2340.
576 https://doi.org/10.1175/2010JAS3433.1
577 Chang, K.-W., & L'Ecuyer, T. (2020). Influence of gravity wave temperature anomalies and
578 their vertical gradients on cirrus clouds in the tropical tropopause layer – a satellite-based
579 view. *Atmospheric Chemistry and Physics*, *20*(21), 12499–12514.
580 https://doi.org/10.5194/acp-20-12499-2020
581 Chiodo, G., Polvani, L. M., Marsh, D. R., Stenke, A., Ball, W., Rozanov, E., et al. (2018). The
582 Response of the Ozone Layer to Quadrupled CO2 Concentrations. *Journal of Climate*,
583 *31*(10), 3893–3907. https://doi.org/10.1175/JCLI-D-17-0492.1
584 Corti, T., Luo, B. P., Fu, Q., Vomel, H., & Peter, T. (2006). The impact of cirrus clouds on
585 tropical troposphere-to-stratosphere transport. *Atmos. Chem. Phys.*, 9.
586 Das, S. S., & Suneeth, K. V. (2020). Seasonal and interannual variations of water vapor in the
587 upper troposphere and lower stratosphere over the Asian Summer Monsoon region- in
588 perspective of the tropopause and ocean-atmosphere interactions. *Journal of Atmospheric*
589 *and Solar-Terrestrial Physics*, *201*, 105244. https://doi.org/10.1016/j.jastp.2020.105244
590 Davis, S. M., Liang, C. K., & Rosenlof, K. H. (2013). Interannual variability of tropical
591 tropopause layer clouds. *Geophysical Research Letters*, *40*(11), 2862–2866.
592 https://doi.org/10.1002/grl.50512

593 Dessler, A. E., Schoeberl, M. R., Wang, T., Davis, S. M., & Rosenlof, K. H. (2013).
594 Stratospheric water vapor feedback. *Proceedings of the National Academy of Sciences*,
595 *110*(45), 18087–18091. https://doi.org/10.1073/pnas.1310344110
596 Dessler, A. E., Schoeberl, M. R., Wang, T., Davis, S. M., Rosenlof, K. H., & Vernier, J.-P.
597 (2014). Variations of stratospheric water vapor over the past three decades. *Journal of*
598 *Geophysical Research: Atmospheres*, *119*(22), 12,588-12,598.
599 https://doi.org/10.1002/2014JD021712
600 Diallo, M., Riese, M., Birner, T., Konopka, P., Müller, R., Hegglin, M. I., et al. (2018). Response
601 of stratospheric water vapor and ozone to the unusual timing of El Niño and the QBO
602 disruption in 2015–2016. *Atmospheric Chemistry and Physics*, *18*(17), 13055–13073.
603 https://doi.org/10.5194/acp-18-13055-2018
604 Ding, Q., & Fu, Q. (2018). A warming tropical central Pacific dries the lower stratosphere.
605 *Climate Dynamics*, *50*(7), 2813–2827. https://doi.org/10.1007/s00382-017-3774-y
606 Dinh, T. P., Durran, D. R., & Ackerman, T. P. (2010). Maintenance of tropical tropopause layer
607 cirrus. *Journal of Geophysical Research: Atmospheres*, *115*(D2).
608 https://doi.org/10.1029/2009JD012735
609 Eguchi, N., & Kodera, K. (2010). Impacts of Stratospheric Sudden Warming Event on Tropical
610 Clouds and Moisture Fields in the TTL: A Case Study. *Sola*, *6*, 137–140.
611 https://doi.org/10.2151/sola.2010-035
612 de F. Forster, P. M., & Shine, K. P. (1999). Stratospheric water vapour changes as a possible
613 contributor to observed stratospheric cooling. *Geophysical Research Letters*, *26*(21), 3309–
614 3312. https://doi.org/10.1029/1999GL010487

615 Flury, T., Wu, D. L., & Read, W. G. (2012). Correlation among cirrus ice content, water vapor
616 and temperature in the TTL as observed by CALIPSO and Aura/MLS. *Atmospheric*
617 *Chemistry and Physics*, *12*(2), 683–691. https://doi.org/10.5194/acp-12-683-2012
618 Flury, Thomas, wu, D., & Read, W. (2012). Variability of the Brewer-Dobson circulation's
619 meridional and vertical branch using Aura/MLS water vapor. *Atmospheric Chemistry &*
620 *Physics Discussions*, *12*, 21291–21320. https://doi.org/10.5194/acpd-12-21291-2012
621 Fu, Q. (2013). Bottom up in the tropics. *Nature Climate Change*, *3*(11), 957–958.
622 https://doi.org/10.1038/nclimate2039
623 Fu, Q., Hu, Y., & Yang, Q. (2007). Identifying the top of the tropical tropopause layer from
624 vertical mass flux analysis and CALIPSO lidar cloud observations. *Geophysical Research*
625 *Letters*, *34*(14). https://doi.org/10.1029/2007GL030099
626 Fu, Q., Smith, M., & Yang, Q. (2018). The Impact of Cloud Radiative Effects on the Tropical
627 Tropopause Layer Temperatures. *Atmosphere*, *9*(10), 377.
628 https://doi.org/10.3390/atmos9100377
629 Fu, Q., Wang, M., White, R. H., Pahlavan, H. A., Alexander, B., & Wallace, J. M. (2020). Quasi-
630 Biennial Oscillation and Sudden Stratospheric Warmings during the Last Glacial
631 Maximum. *Atmosphere*, *11*(9), 943. https://doi.org/10.3390/atmos11090943
632 Fueglistaler, S., & Haynes, P. H. (2005). Control of interannual and longer-term variability of
633 stratospheric water vapor. *Journal of Geophysical Research: Atmospheres*, *110*(D24).
634 https://doi.org/10.1029/2005JD006019
635 Fueglistaler, S., Dessler, A. E., Dunkerton, T. J., Folkins, I., Fu, Q., & Mote, P. W. (2009).
636 Tropical tropopause layer. *Reviews of Geophysics*, *47*(1).
637 https://doi.org/10.1029/2008RG000267

638 Garfinkel, C. I., & Hartmann, D. L. (2008). Different ENSO teleconnections and their effects on
639 the stratospheric polar vortex. *Journal of Geophysical Research: Atmospheres*, *113*(D18).
640 https://doi.org/10.1029/2008JD009920
641 Garfinkel, C. I., Waugh, D. W., Oman, L. D., Wang, L., & Hurwitz, M. M. (2013). Temperature
642 trends in the tropical upper troposphere and lower stratosphere: Connections with sea
643 surface temperatures and implications for water vapor and ozone. *Journal of Geophysical*
644 *Research: Atmospheres*, *118*(17), 9658–9672. https://doi.org/10.1002/jgrd.50772
645 Garfinkel, Chaim I., Harari, O., Ziskin Ziv, S., Rao, J., Morgenstern, O., Zeng, G., et al. (2021).
646 Influence of the El Niño–Southern Oscillation on entry stratospheric water vapor in coupled
647 chemistry–ocean CCMI and CMIP6 models. *Atmospheric Chemistry and Physics*, *21*(5),
648 3725–3740. https://doi.org/10.5194/acp-21-3725-2021
649 Get[TEL]man, A., & Forster, P. M. de F. (2002). A Climatology of the Tropical Tropopause Layer.
650 *Journal of the Meteorological Society of Japan. Ser. II*, *80*(4B), 911–924.
651 https://doi.org/10.2151/jmsj.80.911
652 Gettelman, A., Hegglin, M. I., Son, S.-W., Kim, J., Fujiwara, M., Birner, T., et al. (2010).
653 Multimodel assessment of the upper troposphere and lower stratosphere: Tropics and global
654 trends. *Journal of Geophysical Research: Atmospheres*, *115*(D3).
655 https://doi.org/10.1029/2009JD013638
656 Grise, K. M., & Thompson, D. W. J. (2013). On the Signatures of Equatorial and Extratropical
657 Wave Forcing in Tropical Tropopause Layer Temperatures. *Journal of the Atmospheric*
658 *Sciences*, *70*(4), 1084–1102. https://doi.org/10.1175/JAS-D-12-0163.1
659 Hardiman, S. C., Boutle, I. A., Bushell, A. C., Butchart, N., Cullen, M. J. P., Field, P. R., et al.
660 (2015). Processes Controlling Tropical Tropopause Temperature and Stratospheric Water

Vapor in Climate Models. *Journal of Climate*, *28*(16), 6516–6535. https://doi.org/10.1175/JCLI-D-15-0075.1

Hersbach, H., Bell, B., Berrisford, P., Hirahara, S., Horányi, A., Muñoz-Sabater, J., et al. (2020). The ERA5 global reanalysis. *Quarterly Journal of the Royal Meteorological Society*, *146*(730), 1999–2049. https://doi.org/10.1002/qj.3803

Holloway, C. E., & Neelin, J. D. (2007). The Convective Cold Top and Quasi Equilibrium. *Journal of the Atmospheric Sciences*, *64*(5), 1467–1487. https://doi.org/10.1175/JAS3907.1

Holton, J., & Gettelman, A. (2001). Horizontal transport and dehydration in the stratosphere. *Geophys. Res. Lett.*, *28*, 2799–2802. https://doi.org/10.1029/2001GL013148

Holton, J., Haynes, P., Mcintyre, M., Douglass, A., Rood, R., & Pfister, L. (1995). Stratosphere-Troposphere Exchange. *Reviews of Geophysics - REV GEOPHYS*, *33*. https://doi.org/10.1029/95RG02097

Jensen, E. J., Toon, O. B., Pfister, L., & Selkirk, H. B. (1996). Dehydration of the upper troposphere and lower stratosphere by subvisible cirrus clouds near the tropical tropopause. *Geophysical Research Letters*, *23*(8), 825–828. https://doi.org/10.1029/96GL00722

Jensen, E. J., Diskin, G., Lawson, R. P., Lance, S., Bui, T. P., Hlavka, D., et al. (2013). Ice nucleation and dehydration in the Tropical Tropopause Layer. *Proceedings of the National Academy of Sciences*, *110*(6), 2041–2046. https://doi.org/10.1073/pnas.1217104110

Joshi, M. M., Webb, M. J., Maycock, A. C., & Collins, M. (2010). Stratospheric water vapour and high climate sensitivity in a version of the HadSM3 climate model. *Atmospheric Chemistry and Physics*, *10*(15), 7161–7167. https://doi.org/10.5194/acp-10-7161-2010

682 Kim, J.-E., & Alexander, M. J. (2015). Direct impacts of waves on tropical cold point tropopause
683 temperature. *Geophysical Research Letters*, *42*(5), 1584–1592.
684 https://doi.org/10.1002/2014GL062737
685 Kim, J.-E., Alexander, M. J., Bui, T. P., Dean-Day, J. M., Lawson, R. P., Woods, S., et al.
686 (2016). Ubiquitous influence of waves on tropical high cirrus clouds. *Geophysical Research*
687 *Letters*, *43*(11), 5895–5901. https://doi.org/10.1002/2016GL069293
688 Kirk-Davidoff, D. B., Hintsa, E. J., Anderson, J. G., & Keith, D. W. (1999). The effect of climate
689 change on ozone depletion through changes in stratospheric water vapour. *Nature*,
690 *402*(6760), 399–401. https://doi.org/10.1038/46521
691 Konopka, P., Ploeger, F., Tao, M., & Riese, M. (2016). Zonally resolved impact of ENSO on the
692 stratospheric circulation and water vapor entry values. *Journal of Geophysical Research:*
693 *Atmospheres*, *121*(19), 11,486-11,501. https://doi.org/10.1002/2015JD024698
694 Kuo, Y.-H., Wee, T.-K., Sokolovskiy, S., Rocken, C., Schreiner, W., Hunt, D., & Anthes, R. A.
695 (2004). Inversion and Error Estimation of GPS Radio Occultation Data. *Journal of the*
696 *Meteorological Society of Japan. Ser. II*, *82*(1B), 507–531.
697 https://doi.org/10.2151/jmsj.2004.507
698 Kursinski, E. R., Hajj, G. A., Schofield, J. T., Linfield, R. P., & Hardy, K. R. (1997). Observing
699 Earth's atmosphere with radio occultation measurements using the Global Positioning
700 System. *Journal of Geophysical Research: Atmospheres*, *102*(D19), 23429–23465.
701 https://doi.org/10.1029/97JD01569
702 Li, Y., & Thompson, D. W. J. (2013). The signature of the stratospheric Brewer–Dobson
703 circulation in tropospheric clouds. *Journal of Geophysical Research: Atmospheres*, *118*(9),
704 3486–3494. https://doi.org/10.1002/jgrd.50339

Liang, C. K., Eldering, A., Gettelman, A., Tian, B., Wong, S., Fetzer, E. J., & Liou, K. N. (2011). Record of tropical interannual variability of temperature and water vapor from a combined AIRS-MLS data set. *Journal of Geophysical Research: Atmospheres*, *116*(D6). https://doi.org/10.1029/2010JD014841

Lin, P., Paynter, D., Ming, Y., & Ramaswamy, V. (2017). Changes of the Tropical Tropopause Layer under Global Warming. *Journal of Climate*, *30*(4), 1245–1258. https://doi.org/10.1175/JCLI-D-16-0457.1

Lindeman, R. H., Merenda, P. F., & Gold, R. Z. (1980). *Introduction to bivariate and multivariate analysis*. Glenview, Ill: Scott, Foresman.

Lorenz, D. J., & DeWeaver, E. T. (2007). Tropopause height and zonal wind response to global warming in the IPCC scenario integrations. *Journal of Geophysical Research: Atmospheres*, *112*(D10). https://doi.org/10.1029/2006JD008087

Lu, J., Xie, F., Sun, C., Luo, J., Cai, Q., Zhang, J., et al. (2020). Analysis of factors influencing tropical lower stratospheric water vapor during 1980–2017. *Npj Climate and Atmospheric Science*, *3*(1), 1–11. https://doi.org/10.1038/s41612-020-00138-7

Luo, J., Hou, J., & Xu, X. (2021). Variations in Stratospheric Gravity Waves Derived from Temperature Observations of Multi-GNSS Radio Occultation Missions. *Remote Sensing*, *13*(23), 4835. https://doi.org/10.3390/rs13234835

Marsh, D. R., & Garcia, R. R. (2007). Attribution of decadal variability in lower-stratospheric tropical ozone. *Geophysical Research Letters*, *34*(21). https://doi.org/10.1029/2007GL030935

726 Martin, Z., Sobel, A., Butler, A., & Wang, S. (2021). Variability in QBO Temperature
727 Anomalies on Annual and Decadal Time Scales. *Journal of Climate*, *34*(2), 589–605.
728 https://doi.org/10.1175/JCLI-D-20-0287.1
729 Match, A., & Gerber, E. P. (2022). Tropospheric Expansion Under Global Warming Reduces
730 Tropical Lower Stratospheric Ozone. *Geophysical Research Letters*, *49*(19),
731 e2022GL099463. https://doi.org/10.1029/2022GL099463
732 McFarquhar, G. M., Heymsfield, A. J., Spinhirne, J., & Hart, B. (2000). Thin and Subvisual
733 Tropopause Tropical Cirrus: Observations and Radiative Impacts. *Journal of the*
734 *Atmospheric Sciences*, *57*(12), 1841–1853. https://doi.org/10.1175/1520-
735 0469(2000)057<1841:TASTTC>2.0.CO;2
736 Mote, P. W., Rosenlof, K. H., McIntyre, M. E., Carr, E. S., Gille, J. C., Holton, J. R., et al.
737 (1996). An atmospheric tape recorder: The imprint of tropical tropopause temperatures on
738 stratospheric water vapor. *Journal of Geophysical Research: Atmospheres*, *101*(D2), 3989–
739 4006. https://doi.org/10.1029/95JD03422
740 Ortland, D. A., & Alexander, M. J. (2014). The Residual-Mean Circulation in the Tropical
741 Tropopause Layer Driven by Tropical Waves. *Journal of the Atmospheric Sciences*, *71*(4),
742 1305–1322. https://doi.org/10.1175/JAS-D-13-0100.1
743 Pahlavan, H. A., Fu, Q., Wallace, J. M., & Kiladis, G. N. (2021). Revisiting the Quasi-Biennial
744 Oscillation as Seen in ERA5. Part I: Description and Momentum Budget. *Journal of the*
745 *Atmospheric Sciences*, *78*(3), 673–691. https://doi.org/10.1175/JAS-D-20-0248.1
746 Philander, G. (1990). Geophysical Interplays: *El Niño, La Niña, and the Southern Oscillation* . S.
747 George Philander. Academic Press, San Diego, CA, 1989. x, 293 pp., illus. $59.50.

International Geophysics Series, vol. 46. *Science*, *248*(4957), 904–905. https://doi.org/10.1126/science.248.4957.904

Plumb, R. A., & Bell, R. C. (1982). A model of the quasi-biennial oscillation on an equatorial beta-plane. *Quarterly Journal of the Royal Meteorological Society*, *108*(456), 335–352. https://doi.org/10.1002/qj.49710845604

Plumb, R. A., & Eluszkiewicz, J. (1999). The Brewer–Dobson Circulation: Dynamics of the Tropical Upwelling. *Journal of the Atmospheric Sciences*, *56*(6), 868–890. https://doi.org/10.1175/1520-0469(1999)056<0868:TBDCDO>2.0.CO;2

Podglajen, A., Hertzog, A., Plougonven, R., & Legras, B. (2016). Lagrangian temperature and vertical velocity fluctuations due to gravity waves in the lower stratosphere. *Geophysical Research Letters*, *43*(7), 3543–3553. https://doi.org/10.1002/2016GL068148

Podglajen, A., Plougonven, R., Hertzog, A., & Jensen, E. (2018). Impact of gravity waves on the motion and distribution of atmospheric ice particles. *Atmospheric Chemistry and Physics*, *18*(14), 10799–10823. https://doi.org/10.5194/acp-18-10799-2018

Randel, W., & Park, M. (2019). Diagnosing Observed Stratospheric Water Vapor Relationships to the Cold Point Tropical Tropopause. *Journal of Geophysical Research: Atmospheres*, *124*(13), 7018–7033. https://doi.org/10.1029/2019JD030648

Randel, W. J., & Jensen, E. J. (2013). Physical processes in the tropical tropopause layer and their roles in a changing climate. *Nature Geoscience*, *6*(3), 169–176. https://doi.org/10.1038/ngeo1733

Randel, W. J., & Wu, F. (2015). Variability of Zonal Mean Tropical Temperatures Derived from a Decade of GPS Radio Occultation Data. *Journal of the Atmospheric Sciences*, *72*(3), 1261–1275. https://doi.org/10.1175/JAS-D-14-0216.1

771 Randel, W. J., Wu, F., & Gaffen, D. J. (2000). Interannual variability of the tropical tropopause
772 derived from radiosonde data and NCEP reanalyses. *Journal of Geophysical Research:*
773 *Atmospheres*, *105*(D12), 15509–15523. https://doi.org/10.1029/2000JD900155
774 Randel, W. J., Garcia, R. R., Calvo, N., & Marsh, D. (2009). ENSO influence on zonal mean
775 temperature and ozone in the tropical lower stratosphere. *Geophysical Research Letters*,
776 *36*(15). https://doi.org/10.1029/2009GL039343
777 Randel, W. J., Park, M., Emmons, L., Kinnison, D., Bernath, P., Walker, K. A., et al. (2010).
778 Asian Monsoon Transport of Pollution to the Stratosphere. *Science*, *328*(5978), 611–613.
779 https://doi.org/10.1126/science.1182274
780 Rosenlof, K. H. (1995). Seasonal cycle of the residual mean meridional circulation in the
781 stratosphere. *Journal of Geophysical Research*, *100*, 5173–5191.
782 https://doi.org/10.1029/94JD03122
783 Santer, B. D., Sausen, R., Wigley, T. M. L., Boyle, J. S., AchutaRao, K., Doutriaux, C., et al.
784 (2003). Behavior of tropopause height and atmospheric temperature in models, reanalyses,
785 and observations: Decadal changes. *Journal of Geophysical Research: Atmospheres*,
786 *108*(D1), ACL 1-1-ACL 1-22. https://doi.org/10.1029/2002JD002258
787 Scherllin-Pirscher, B., Deser, C., Ho, S.-P., Chou, C., Randel, W., & Kuo, Y.-H. (2012). The
788 vertical and spatial structure of ENSO in the upper troposphere and lower stratosphere from
789 GPS radio occultation measurements. *Geophysical Research Letters*, *39*(20).
790 https://doi.org/10.1029/2012GL053071
791 Sokol, A. B., & Hartmann, D. L. (2020). Tropical Anvil Clouds: Radiative Driving Toward a
792 Preferred State. *Journal of Geophysical Research: Atmospheres*, *125*(21), e2020JD033107.
793 https://doi.org/10.1029/2020JD033107

794 Solomon, S., Rosenlof, K. H., Portmann, R. W., Daniel, J. S., Davis, S. M., Sanford, T. J., &
795 Plattner, G.-K. (2010). Contributions of Stratospheric Water Vapor to Decadal Changes in
796 the Rate of Global Warming. *Science*, *327*(5970), 1219–1223.
797 https://doi.org/10.1126/science.1182488
798 Sunilkumar, S. V., Parameswaran, K., Rajeev, K., Krishna Murthy, B. V., Meenu, S., Mehta, S.
799 K., & Babu, A. (2010). Semitransparent cirrus clouds in the tropical tropopause layer during
800 two contrasting seasons. *Journal of Atmospheric and Solar-Terrestrial Physics*, *72*(9), 745–
801 762. https://doi.org/10.1016/j.jastp.2010.03.020
802 Sweeney, A., Fu, Q., Pahlavan, H. A., & Haynes, P. (2023). Seasonality of the QBO Impact on
803 Equatorial Clouds. *Journal of Geophysical Research: Atmospheres*, *128*(7),
804 e2022JD037737. https://doi.org/10.1029/2022JD037737
805 Sweeney, A. J., & Fu, Q. (2021). Diurnal Cycles of Synthetic Microwave Sounding Lower-
806 Stratospheric Temperatures from Radio Occultation Observations, Reanalysis, and Model
807 Simulations. *Journal of Atmospheric and Oceanic Technology*, *38*(12), 2045–2059.
808 https://doi.org/10.1175/JTECH-D-21-0071.1
809 Tegtmeier, S., Anstey, J., Davis, S., Ivanciu, I., Jia, Y., McPhee, D., & Pilch Kedzierski, R.
810 (2020). Zonal Asymmetry of the QBO Temperature Signal in the Tropical Tropopause
811 Region. *Geophysical Research Letters*, *47*(24), e2020GL089533.
812 https://doi.org/10.1029/2020GL089533
813 Thornberry, T. D., Rollins, A. W., Avery, M. A., Woods, S., Lawson, R. P., Bui, T. V., & Gao,
814 R.-S. (2017). Ice water content-extinction relationships and effective diameter for TTL
815 cirrus derived from in situ measurements during ATTREX 2014. *Journal of Geophysical*
816 *Research: Atmospheres*, *122*(8), 4494–4507. https://doi.org/10.1002/2016JD025948

817 Thorsen, T. J., Fu, Q., Comstock, J. M., Sivaraman, C., Vaughan, M. A., Winker, D. M., &
818 Turner, D. D. (2013). Macrophysical properties of tropical cirrus clouds from the CALIPSO
819 satellite and from ground-based micropulse and Raman lidars. *Journal of Geophysical*
820 *Research: Atmospheres*, *118*(16), 9209–9220. https://doi.org/10.1002/jgrd.50691
821 Tian, E. W., Su, H., Tian, B., & Jiang, J. H. (2019). Interannual variations of water vapor in the
822 tropical upper troposphere and the lower and middle stratosphere and their connections to
823 ENSO and QBO. *Atmospheric Chemistry and Physics*, *19*(15), 9913–9926.
824 https://doi.org/10.5194/acp-19-9913-2019
825 de la Torre, A., Schmidt, T., & Wickert, J. (2006). A global analysis of wave potential energy in
826 the lower stratosphere derived from 5 years of GPS radio occultation data with CHAMP.
827 *Geophysical Research Letters*, *33*(24). https://doi.org/10.1029/2006GL027696
828 Tseng, H. -H., & Fu, Q. (2017). Tropical tropopause layer cirrus and its relation to tropopause.
829 *Journal of Quantitative Spectroscopy and Radiative Transfer*, *188*, 118–131.
830 https://doi.org/10.1016/j.jqsrt.2016.05.029
831 Tseng, Hsiu-Hui, & Fu, Q. (2017). Temperature Control of the Variability of Tropical
832 Tropopause Layer Cirrus Clouds. *Journal of Geophysical Research: Atmospheres*, *122*(20),
833 11,062-11,075. https://doi.org/10.1002/2017JD027093
834 Tsuda, T., Nishida, M., Rocken, C., & Ware, R. H. (2000a). A Global Morphology of Gravity
835 Wave Activity in the Stratosphere Revealed by the GPS Occultation Data (GPS/MET).
836 *Journal of Geophysical Research: Atmospheres*, *105*(D6), 7257–7273.
837 https://doi.org/10.1029/1999JD901005
838 Tsuda, T., Nishida, M., Rocken, C., & Ware, R. H. (2000b). A Global Morphology of Gravity
839 Wave Activity in the Stratosphere Revealed by the GPS Occultation Data (GPS/MET).

Journal of Geophysical Research: Atmospheres, *105*(D6), 7257–7273. https://doi.org/10.1029/1999JD901005

Tweedy, O. V., Waugh, D. W., Randel, W. J., Abalos, M., Oman, L. D., & Kinnison, D. E. (2018). The Impact of Boreal Summer ENSO Events on Tropical Lower Stratospheric Ozone. *Journal of Geophysical Research: Atmospheres*, *123*(17), 9843–9857. https://doi.org/10.1029/2018JD029020

Ueyama, R., Jensen, E. J., Pfister, L., & Kim, J.-E. (2015). Dynamical, convective, and microphysical control on wintertime distributions of water vapor and clouds in the tropical tropopause layer. *Journal of Geophysical Research: Atmospheres*, *120*(19), 10,483-10,500. https://doi.org/10.1002/2015JD023318

Ueyama, R., Jensen, E. J., & Pfister, L. (2018). Convective Influence on the Humidity and Clouds in the Tropical Tropopause Layer During Boreal Summer. *Journal of Geophysical Research: Atmospheres*, *123*(14), 7576–7593. https://doi.org/10.1029/2018JD028674

Ventrice, M., Wheeler, M., Hendon, H., Iii, S., Thorncroft, C., & Kiladis, G. (2013). A Modified Multivariate Madden-Julian Oscillation Index Using Velocity Potential. *Monthly Weather Review*, *141*, 4197–4210. https://doi.org/10.1175/MWR-D-12-00327.1

Virts, K. S., & Wallace, J. M. (2014). Observations of Temperature, Wind, Cirrus, and Trace Gases in the Tropical Tropopause Transition Layer during the MJO. *Journal of the Atmospheric Sciences*, *71*(3), 1143–1157. https://doi.org/10.1175/JAS-D-13-0178.1

Virts, K. S., Wallace, J. M., Fu, Q., & Ackerman, T. P. (2010). Tropical Tropopause Transition Layer Cirrus as Represented by CALIPSO Lidar Observations. *Journal of the Atmospheric Sciences*, *67*(10), 3113–3129. https://doi.org/10.1175/2010JAS3412.1

862 Walker, J. M., Bordoni, S., & Schneider, T. (2015). Interannual Variability in the Large-Scale
863 Dynamics of the South Asian Summer Monsoon. *Journal of Climate*, *28*(9), 3731–3750.
864 https://doi.org/10.1175/JCLI-D-14-00612.1
865 Wang, L., & Alexander, M. J. (2010). Global estimates of gravity wave parameters from GPS
866 radio occultation temperature data. *Journal of Geophysical Research: Atmospheres*,
867 *115*(D21). https://doi.org/10.1029/2010JD013860
868 Wang, M., & Fu, Q. (2021). Stratosphere-Troposphere Exchange of Air Masses and Ozone
869 Concentrations Based on Reanalyses and Observations. *Journal of Geophysical Research:*
870 *Atmospheres*, *126*(18), e2021JD035159. https://doi.org/10.1029/2021JD035159
871 Wang, T., Wu, D. L., Gong, J., & Tsai, V. (2019). Tropopause Laminar Cirrus and Its Role in the
872 Lower Stratosphere Total Water Budget. *Journal of Geophysical Research: Atmospheres*,
873 *124*(13), 7034–7052. https://doi.org/10.1029/2018JD029845
874 Winker, D. M., Pelon, J., Coakley, J. A., Ackerman, S. A., Charlson, R. J., Colarco, P. R., et al.
875 (2010). The CALIPSO Mission: A Global 3D View of Aerosols and Clouds. *Bulletin of the*
876 *American Meteorological Society*, *91*(9), 1211–1230.
877 https://doi.org/10.1175/2010BAMS3009.1
878 Yamazaki, K., Nakamura, T., Ukita, J., & Hoshi, K. (2020). A tropospheric pathway of the
879 stratospheric quasi-biennial oscillation (QBO) impact on the boreal winter polar vortex.
880 *Atmospheric Chemistry and Physics*, *20*(8), 5111–5127. https://doi.org/10.5194/acp-20-
881 5111-2020
882 Yang, Q., Fu, Q., & Hu, Y. (2010). Radiative impacts of clouds in the tropical tropopause layer.
883 *Journal of Geophysical Research: Atmospheres*, *115*(D4).
884 https://doi.org/10.1029/2009JD012393

885 Ye, H., Dessler, A. E., & Yu, W. (2018). Effects of convective ice evaporation on interannual
886 variability of tropical tropopause layer water vapor. *Atmospheric Chemistry and Physics*,
887 *18*(7), 4425–4437. https://doi.org/10.5194/acp-18-4425-2018
888 Zeng, Z., Sokolovskiy, S., Schreiner, W. S., & Hunt, D. (2019). Representation of Vertical
889 Atmospheric Structures by Radio Occultation Observations in the Upper Troposphere and
890 Lower Stratosphere: Comparison to High-Resolution Radiosonde Profiles. *Journal of*
891 *Atmospheric and Oceanic Technology*, *36*(4), 655–670. https://doi.org/10.1175/JTECH-D-
892 18-0105.1
893 Zhou, C., Dessler, A. E., Zelinka, M. D., Yang, P., & Wang, T. (2014). Cirrus feedback on
894 interannual climate fluctuations. *Geophysical Research Letters*, *41*(24), 9166–9173.
895 https://doi.org/10.1002/2014GL062095
896 Ziskin Ziv, S., Garfinkel, C. I., Davis, S., & Banerjee, A. (2022). The roles of the Quasi-Biennial
897 Oscillation and El Niño for entry stratospheric water vapor in observations and coupled
898 chemistry–ocean CCMI and CMIP6 models. *Atmospheric Chemistry and Physics*, *22*(11),
899 7523–7538. https://doi.org/10.5194/acp-22-7523-2022

900
901